CONF-770958--1

HEDL-SA-1268

IN-REACTOR BEHAVIOR OF MATERIALS USED TO CONTROL FUEL-CLADDING CHEMICAL INTERACTION

MASTER

C.N. Wilson, R.L. Gibby, L.A. Lawrence, E.T. Weber

August 22, 1977

Hanford Engineering Development Laboratory
Westinghouse Hanford Company
Richland, Washington

IN-REACTOR BEHAVIOR OF MATERIALS USED TO CONTROL FUEL-CLADDING CHEMICAL INTERACTION

C. N. Wilson, R. L. Gibby, L. A. Lawrence, E. T. Weber

1.0 INTRODUCTION

Fuel-cladding chemical interaction (FCCI) has been recognized as an important factor in the ability to achieve goal burnups in FFTF and future breeder reactor demonstration plants ($\sim$ 8 atom percent and > 10 atom percent respectively), while maintaining sodium outlet temperatures of approximately 600°C. Economic incentives for controlling FCCI include: potential for higher fuel burnup, and increased breeding ratio. One mil (25 μm) of cladding wall thickness is estimated to be worth 1% (10,000 MWD/MTM) burnup capability. One mil (25 μm) of cladding replaced by fuel is estimated to be worth 0.02 increase in breeding ratio.

Temperature and oxygen potential at the cladding inner surface appear to be the two most important parameters determining the type and rate of cladding inner surface corrosion. Irradiation experience has indicated that FCCI can be reduced by lowering the coolant outlet temperature and/or fuel O/M. However, lower temperatures will result in losses in overall thermal efficiency and breeding ratio with current designs. Use of low O/M fuel can result in substantial redistribution of fission product Cs to the blanket region, where reaction with UO_2 can lead to swelling and mechanical interaction with the cladding. Controlling oxygen chemistry in the fuel-cladding gap by using oxygen buffer/getter materials may provide a means of controlling FCCI while maintaining high coolant outlet temperatures.

An irradiation experiment has been conducted in EBR-II in order to test placement of oxygen buffer/getter materials into LMFBR fuel pins to control FCCI. Oxygen buffer/getter concepts used in the HEDL P-23 Special Pins test are illustrated in Figure 1. Metallic Nb, V, Ti and Cr fuel pellet circumferential coatings, porous Nb and Ti pellets at the ends of the fuel column, Nb at pellet interfaces, and V on the cladding inner surface were tested.

In the present paper, selected post-irradiation examination data which provide information about fuel pin chemistry and mechanisms of fuel cladding

chemical interaction are presented. Performance evaluation of candidate concepts for control of FCCI is not intended.

Oxygen Potential

Applicable thermodynamic data and mechanisms hypothesized for austenetic stainless steel corrosion will be briefly reviewed before discussing the fuel pin examination results. With the exception of Cr, the buffer/getter materials tested exhibit several sequential oxidation states with increasing oxygen potential (Figures 2, 3, 4). At a given temperature, the equilibrium between a metal oxide and its next higher oxide occurs at a unique oxygen potential ($\Delta\bar{G}o_2 = RT\ln Po_2$). Therefore, the buffer/getter materials can serve as local oxygen potential indicators in the fuel pin.

Of cladding components, Cr has the lowest threshold for oxidation. The oxidation threshold of 316 stainless steel is the oxygen potential for oxidation of Cr(ss) [$\Delta\bar{G}o_2(600°C) = -140 \frac{kcal}{mole O_2}$ assuming Cr activity of 0.17]. Oxidation rate is limited by oxygen diffusion through the adherent of Cr_2O_3 passive layer. Matrix attack by oxidation requires both a minimum oxygen potential and other environmental factors which destabilize the Cr_2O_3 passive layer.

Intergranular attack is thought to be initiated by oxidation of chrome carbides which precipitate at grain boundaries at irradiation temperatures, exposing adjacent Cr depleted metal for further attack. The $\Delta\bar{G}o_2$ threshold for oxidation of chrome carbides to Cr_2O_3 + C is in the -134 to -138 kcal/mole O_2 range at 600°C depending upon the chrome carbide stoichiometry (i.e. $Cr_{23}C_6$, Cr_7C_3, Cr_3C_2, etc.). Oxidation thresholds for chrome carbides are a few Kcal/mole O_2 higher than for Cr(ss). Without adherent passive layer formation, reaction rate is limited by oxygen transport to exposed grain boundary carbides. Carbon released during carbide oxidation would be free to reform chrome carbides until Cr depletion has occurred in the intergranular region. At higher oxygen potentials [$\Delta\bar{G}o_2(600°C) > -100 \frac{Kcal}{Mole\ O_2}$], oxidation of exposed intergranular carbides to Cr_2O_3 and CO/CO_2 may cause removal of C from intergranular attack regions limiting the extent of intergranular attack at higher $\Delta\bar{G}o_2$ values.

Fuel Pin Examination Results

Control Pin

Pin P-23B-S1 did not contain any oxygen buffer/getter materials and serves as a control pin for the 2.2 atom percent burnup P-23B Special Pins. All P-23B Special Pins were fabricated using 25% PuO_2 mixed-oxide fuel with 65% enriched UO_2 and initial O/M = 1.985 ± 0.005. Radial oxygen redistribution during irradiation was expected to raise the fuel O/M at the fuel surface providing a sufficient oxygen potential to allow matrix attack to occur in the absence of oxygen buffers. Matrix attack was observed in the upper three metallographic sections from P-23B-S1 as shown in Figure 5. No significant cladding attack occurred at the lower metallographic section where the peak cladding inner surface temperature was calculated to be 510°C. No regions of intergranular attack were observed in the control pin.

Nb-Coated Fuel

The nature of cladding attack and distribution of fission product Cs were significantly affected by the presence of Nb-coated fuel. Five observations from fuel pins containing Nb-coated fuel are presented:

1) Fission product Cs redistributed toward Nb-coated fuel,
2) Nb oxidized forming multiphase fuel-cladding interface layers,
3) No cladding matrix attack occurred adjacent to Nb-coated fuel,
4) Localized intergranular attack occurred adjacent to oxidized Nb which had combined with fission product Cs, and
5) No cladding attack occurred with adequate inventory and dispersal of Nb in the fuel column.

Redistribution of fission product Cs is shown for three fuel pins containing Nb in Figure 6. (Zr^{95} gamma scans are proportional to local burnup and delineate the ends of the fuel columns in Figure 6). Pin P-23B-A3 contained two sections of Nb-coated fuel, which are bracketed by the Cs gamma scan peaks (top, Figure 6). Pin P-23B-A5 contained alternating layers of Nb-coated fuel and uncoated fuel. Pin P-23B-B5 contained Nb at each pellet interface. In each case,

redistribution of fission product Cs towards Nb occurred.

Fuel column configuration and selected fuel-cladding interface micrographs for pin P-23B-A3 are shown in Figure 7. No matrix attack is visible adjacent to Nb-coated fuel. In the 178 mm and 337 mm sections, matrix attack comparable to that observed at similar fuel column positions in the control pin occurred. Also note that the 337 mm section is immediately below a porous Ti end pellet, indicating that the end pellet was ineffective in controlling matrix attack.

The irradiated Nb fuel coatings varied in reflectivity appearing bright, grey, or dark grey. Bright fuel coating layers are postulated to be Nb metal, the grey coatings NbO_x (Nb oxides) and the darkest areas NbO_x which had reacted with Cs forming a cesium niobate phase such as $CsNbO_3$. Electron microprobe and Cs gamma scan data supported this postulate. Electron microprobe step scans for Nb indicated a decrease in Nb concentration going across phase boundaries from lighter to darker appearing phases. Electron microprobe line profiles for Cs and Nb across grey appearing and dark appearing fuel coating layers in the 274 mm section are shown in Figure 8. Neither matrix or intergranular attack was observed adjacent to the bright or intermediate grey Nb interface layers. Localized intergranular attack was observed in the 274 mm section adjacent to cesium niobate interface layers (not shown in Figure 7).

Fuel column configuration and selected fuel-cladding interface micrographs for pin P-23B-A5 are shown in Figure 9. No matrix attack comparable to that in the control pin was observed in P-23B-A5. Better dispersal of Nb over the fuel column most likely accounts for the inhibition of matrix attack. A phase boundary, which is postulated to be a Nb-NbO boundary, is visible in the 190 mm section micrograph. At 590°C, $\Delta\overline{G}o_2$ at a Nb-NbO boundary would be approximately -160 Kcal/mole O_2. Intergranular attack to a depth of 2 mills (50 μm) was observed adjacent to the upper Nb-coated fuel layer where Nb had combined with fission product Cs. Electron microprobe examination (Figure 10) revealed an apparent cesium niobate phase present in the intergranular penetrations and continuous with cesium niobate in the fuel cladding gap.

In pin P-23B-B5, which was fabricated with approximately 25 microns of Nb at each fuel pellet interface and was irradiated to 2.2% burnup, no significant cladding attack occurred. The apparent increase in effectiveness of niobium when placed on fuel pellet ends (relative to partial column circumferential placement) was attributed to two factors. First, pellet end coatings gave better dispersal of the Nb throughout the fuel pin that did short sections of circumferential coated fuel, resulting in shorter oxygen diffusion paths. Secondly, the pellet end coatings operated at a higher temperature than the circumferential coatings allowing the oxygen to be gettered more efficiently due to improved kinetics. If all the Nb in P-23B-B5 pellet end coatings oxidized to Nb_2O_5, average fuel O/M would be reduced by 0.025. Reduction of initial fuel O/M from 1.98 to 1.955 would also be expected to result in reduced cladding attack. Niobium migrated radially forming rings of Nb-O-Cs containing phases concentric with the fuel pin axis and located in the outer unrestructured regions of the fuel. Longitudinal sections through two of the reacted Nb interfacial rings are shown in Figure 11. Second phase is visible in the fuel near where the niobium interfacial layers have radially receded. Electron microprobe examination showed no niobium present in restructured regions towards the fuel center.

Ti-Coated Fuel

Fuel pin P-23B-B3 contained alternating layers of Ti-coated and V-coated fuel. Cesium gamma scan data (Figure 12) indicated that Cs redistributed to the Ti-coated fuel. Cesium gettering by the Ti fuel coatings indicates that substantial in-situ oxidation of the Ti coating must have occurred. Of the buffer/getter material tested,only Nb and Ti caused significant redistribution of fission product Cs. Destructive examination has not yet been performed on P-23B-B3.

V-Coated Fuel

Neither ^{137}Cs gamma scanning or electron microprobe examination indicated cesium-vanadium reaction had occurred. Fuel pin P-23C-B5 contained circumferential vanadium coated fuel in the top 210 mm of the fuel column and was irradiated to 30,000 MWD/MTM burnup. As shown by gamma scan data in Figure 12, no significant redistribution of

Cs occurred between the V-coated fuels and the uncoated fuel. Fuel column configuration and metallography at the fuel-cladding interface is shown in Figure 13. No significant cladding attack was observed adjacent to vanadium coated fuel.

Cr-Coated Fuel

Partial oxidation of Cr fuel coatings occurred in the upper (hottest) portion of the fuel pin. Regions of cladding matrix attack (Figure 14) were also found in the upper portion of the pin. The amount of attack was, however, less than observed in the control pin P-23B-S1, or in P-23B-A3 away from Nb fuel coatings. Electron microprobe data indicated Cs reaction with oxidized fuel coating layers. (Figure 15)

Ti and Nb End Pellets

As noted, when discussing pin P-23B-A3, the porous Ti pellets at the ends of the fuel column had no significant affect on fuel cladding chemical interaction. When removed during destructive examination, Ti end pellets appeared bright and identical to their pre-irradiation appearance. The porous Nb end pellets also appeared to have no effect on fuel cladding chemical interaction. However, the Nb end pellets lost their metallic luster and darkened during irradiation.

DISCUSSION

At 600°C, oxygen partial pressure [$Po_2 = \exp\left(\frac{\Delta\bar{G}o_2}{RT}\right)$] at the cladding oxidation threshold is 9.07×10^{-36} atmospheres, or about one O_2 molecule in 13 trillion litres. At 700°C, Po_2 at the cladding oxidation threshold is about 2.4×10^{-31} atmospheres, or one O_2 molecule in 0.5 billion litres. Obviously, for cladding oxidation to occur at or slightly above the thermodynamic oxygen potential threshold, an oxygen transport mechanism must exist. Such a transport mechanism requires interaction (wetting) of the cladding by an oxygen containing phase, or formation of an oxide at the fuel which is volatile at fuel surface temperatures and can be reduced by Cr (ss). A vapor phase transport mechanism which is capable of moving oxygen in the fuel-cladding gap at $\Delta\bar{G}o_2 < -110$ Kcal/mole O_2 is difficult to imagine. At $\Delta Go_2 > -100$ Kcal/mole O_2,

H_2/H_2O, CO/CO_2, and perhaps oxides of Cs and other fission products, can transport oxygen.

Niobium, V and Ti fuel coatings were found to readily oxidize in-situ, indicating solid state oxygen transport from the fuel. (Oxidation of Ti fuel coatings is presumed because of the redistribution of fission product Cs to Ti coated fuel). Where buffer/getter materials were well dispersed in the fuel column, such as with Nb at pellet interfaces, full column of Nb-coated fuel, and V-coated fuel in the top (hottest cladding) 2/3 of the fuel column, cladding attack was controlled. In these cases, the buffer/getter materials were able to buffer fuel oxygen potential below values where vapor phase oxygen transport mechanisms could operate. Fuel surfaces farther removed from buffer/getter coatings may have $\Delta\bar{G}o_2$ sufficient for vapor phase oxygen transport to the cladding. The fuel column and the Ti and Nb end pellets made poor contact compared to the interfaces between fuel and the fuel coatings, requiring vapor phase oxygen transport for oxidation of the Ti and Nb end pellets.

Partial oxidation of Cr fuel coatings were observed in the hotter upper sections of the fuel pin. Oxidation of the Cr-fuel coatings were most likely not sufficient to protect the cladding for the same reasons that the cladding is resistant to oxidation. A Cr_2O_3 passive layer most likely limited oxidation kinetics at the Cr fuel coating until $\Delta\bar{G}o_2$ was sufficient for oxygen transport to the cladding, at which point the cladding and the Cr fuel coating both oxidized at similar rates.

Since Cs vapor is known to be quite aggressive towards most metal oxides at high temperatures, it is probable that Cs may destabilize the cladding Cr_2O_3 passive layer. Below $\Delta\bar{G}o_2$ for formation of Cs_2O or Cs reaction with UO_{2+x}, Cs mobility in the fuel pin is high. Cladding matrix attack in the proximity of a cesium getter may be inhibited by low $\Delta\bar{G}_{Cs}$. A $\Delta\bar{G}_{Cs}$ threshold for accelerated matrix attack would explain intergranular attack without matrix attack, which occurred adjacent to highly oxidized Nb which had combined with Cs. Examination results from this irradiation test indicate that Nb, Cr, and Ti (as oxides) have a greater affinity for Cs in the fuel pin that do V or U (as oxides). In regions where intergranular attack was observed, swelling of the Cs-Nb-O interface layer had caused contact of the interface layer with the cladding. It is postulated that the Cs-Nb-O phase had a $\Delta\bar{G}o_2$ greater than the NbO_2/Nb_2O_5 couple, but below the oxidation threshold for C, and $\Delta\bar{G}_{Cs}$ below the threshold for matrix attack.

CONCLUSIONS

1) Control of fuel-cladding chemical interaction with oxygen buffer/getter materials appears to be feasible.

2) To be effective, oxygen buffer/getter materials must be well dispersed throughout the fuel column.

3) Where effective, buffer/getter materials most likely buffered $\Delta\overline{G}o_2$ to values below which oxygen transport to the cladding could not occur, and not by buffering $\Delta\overline{G}o_2$ below the threshold for oxidation of cladding.

4) Niobium, Cr and most likely Ti, act as Cs getters after oxidation.

REFERENCES

1. U.S. Bureau of Mines Bulletin 542 (1954).
2. U.S. Bureau of Mines Bulletin 605 (1963).
3. O. Kubaschewski, E. L. Evans, C. B. Alcock, Metallurgical Thermochemistry, Pergamon Press, 1967.

LEGEND OF FIGURES

Figure 1 Oxygen potential control concepts used in the HEDL P-23 Special Pins test.

Figure 2 Oxygen potentials for oxidation of Nb and oxidation threshold for cladding.

Figure 3 Oxygen potential for oxidation of V and oxidation threshold for cladding.

Figure 4 Oxygen potential for oxidation of Ti and oxidation threshold for cladding.

Figure 5 Fuel-cladding interfaces from the P-23B-S1 control pin.

Figure 6 Gamma scan data from three fuel pins containing Nb buffer/getter.

Figure 7 Fuel column configuration and fuel-cladding interface micrographs for P-23B-A3.

Figure 8 Electron microprobe traces for Cs and Nb across a grey appearing (in metallography) Nb-oxide layer (above) and across a dark appearing Cs-Nb-O interface layer (below).

Figure 9 Fuel column configuration and fuel-cladding interface micrographs from P-23B-A5.

Figure 10 Electron microprobe rate meter scans showing Cs and Nb in intergranular attack regions in P-23B-A5.

Figure 11 Niobium layers at pellet interfaces in P-23B-B5 after irradiation.

Figure 12 Gamma scan showing Cs redistribution towards Ti-coated fuel in P-23B-B3 (above) and very little Cs redistribution with a partial column of V-coated fuel in P-23C-B5 (below).

Figure 13 Fuel column configuration and fuel-cladding interface micrographs from P-23C-B5.

Figure 14 Behavior of Cr fuel coating at 5 atom percent burnup and approximately 600°C interface temperature, showing localized matrix attack of adjacent cladding.

Figure 15 Electron microprobe data from area shown in Figure 14, indicating Cs-Cr-O reaction.

Figure 16 Conclusions

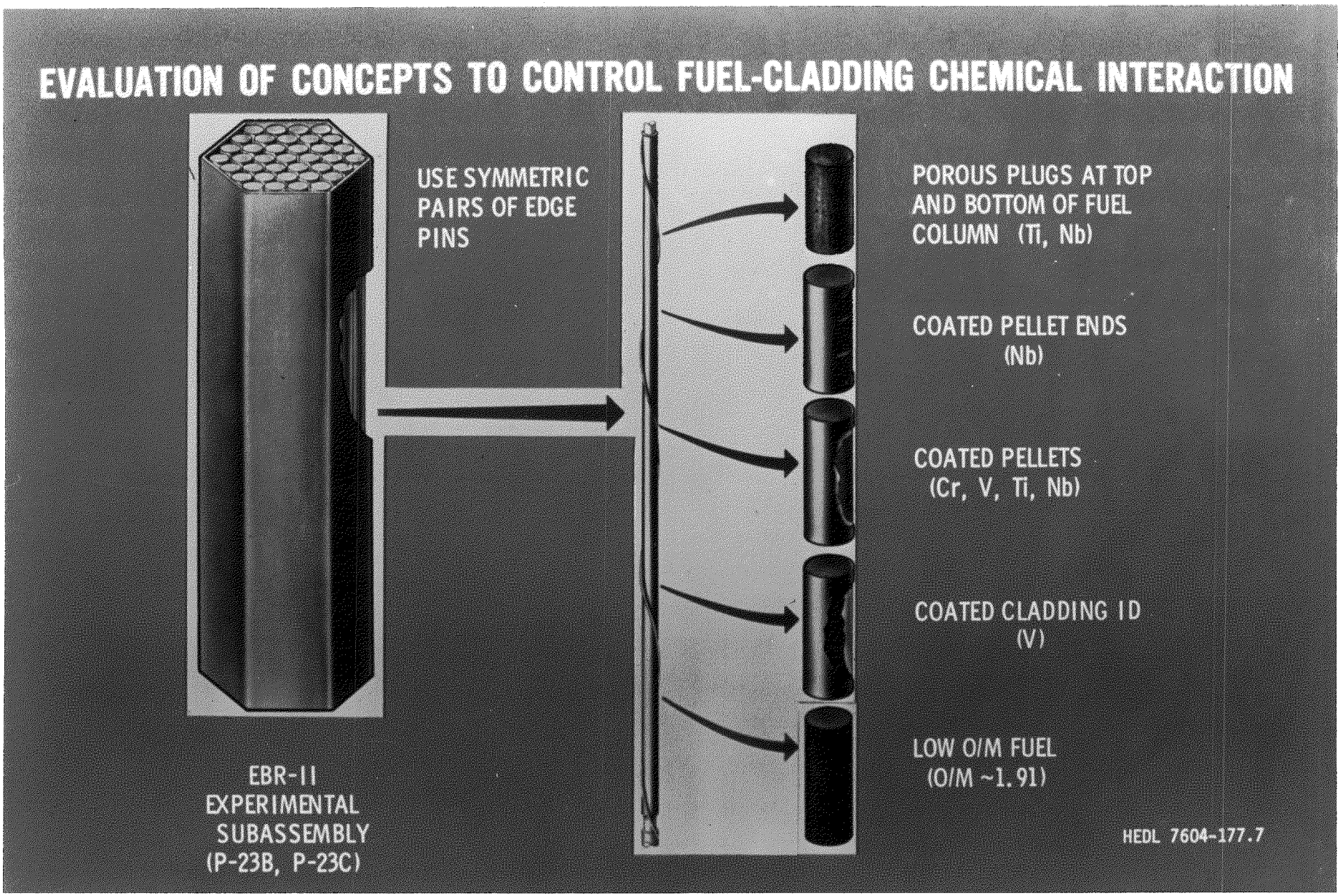
EVALUATION OF CONCEPTS TO CONTROL FUEL-CLADDING CHEMICAL INTERACTION
USE SYMMETRIC PAIRS OF EDGE PINS
POROUS PLUGS AT TOP AND BOTTOM OF FUEL COLUMN (Ti, Nb)
COATED PELLET ENDS (Nb)
COATED PELLETS (Cr, V, Ti, Nb)
COATED CLADDING ID (V)
LOW O/M FUEL (O/M ~1.91)
EBR-II EXPERIMENTAL SUBASSEMBLY (P-23B, P-23C)
HEDL 7604-177.7

FIGURE 1

PHASE BOUNDARY OXYGEN POTENTIAL

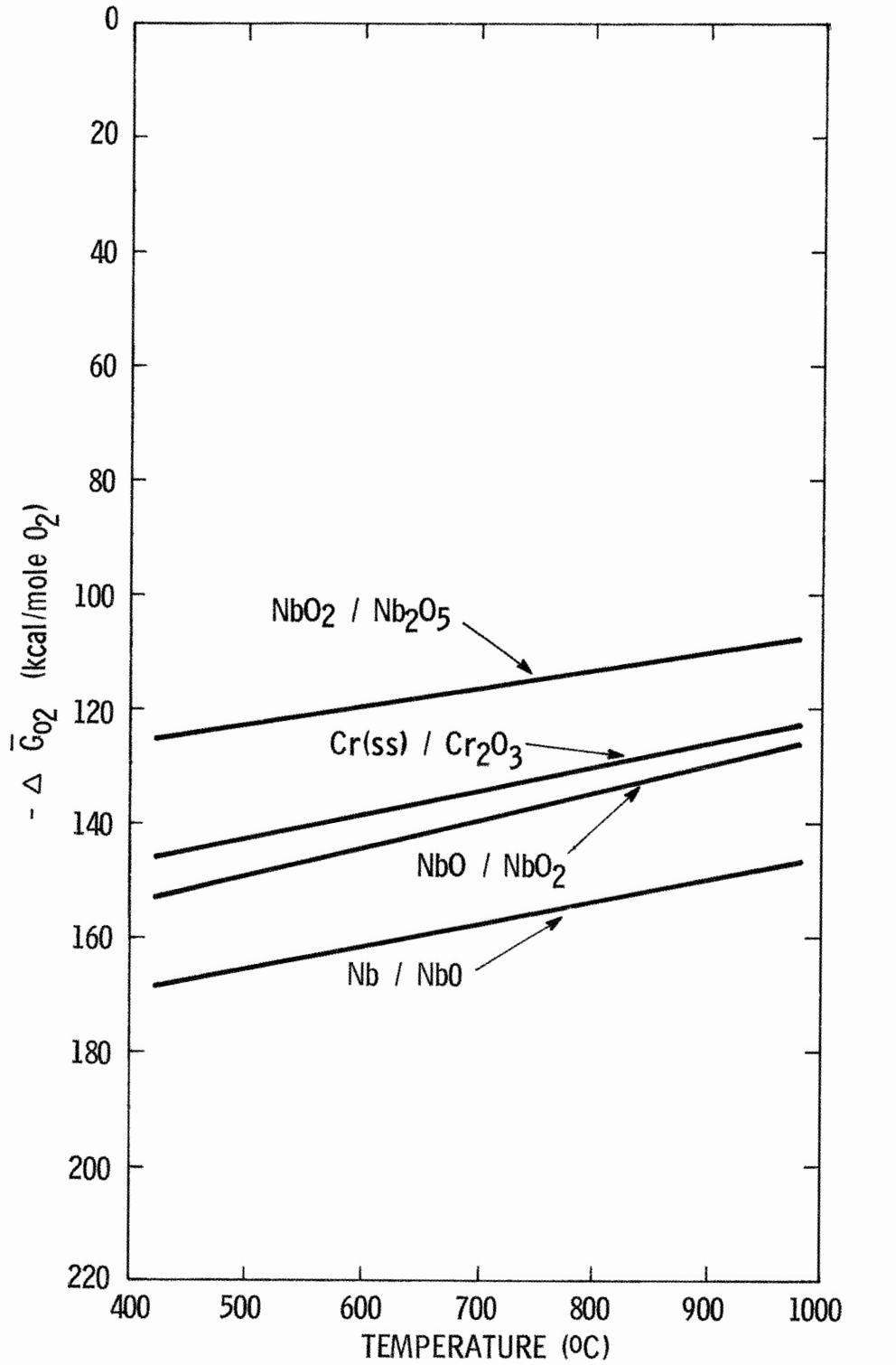

FIGURE 4

PHASE BOUNDARY OXYGEN POTENTIAL

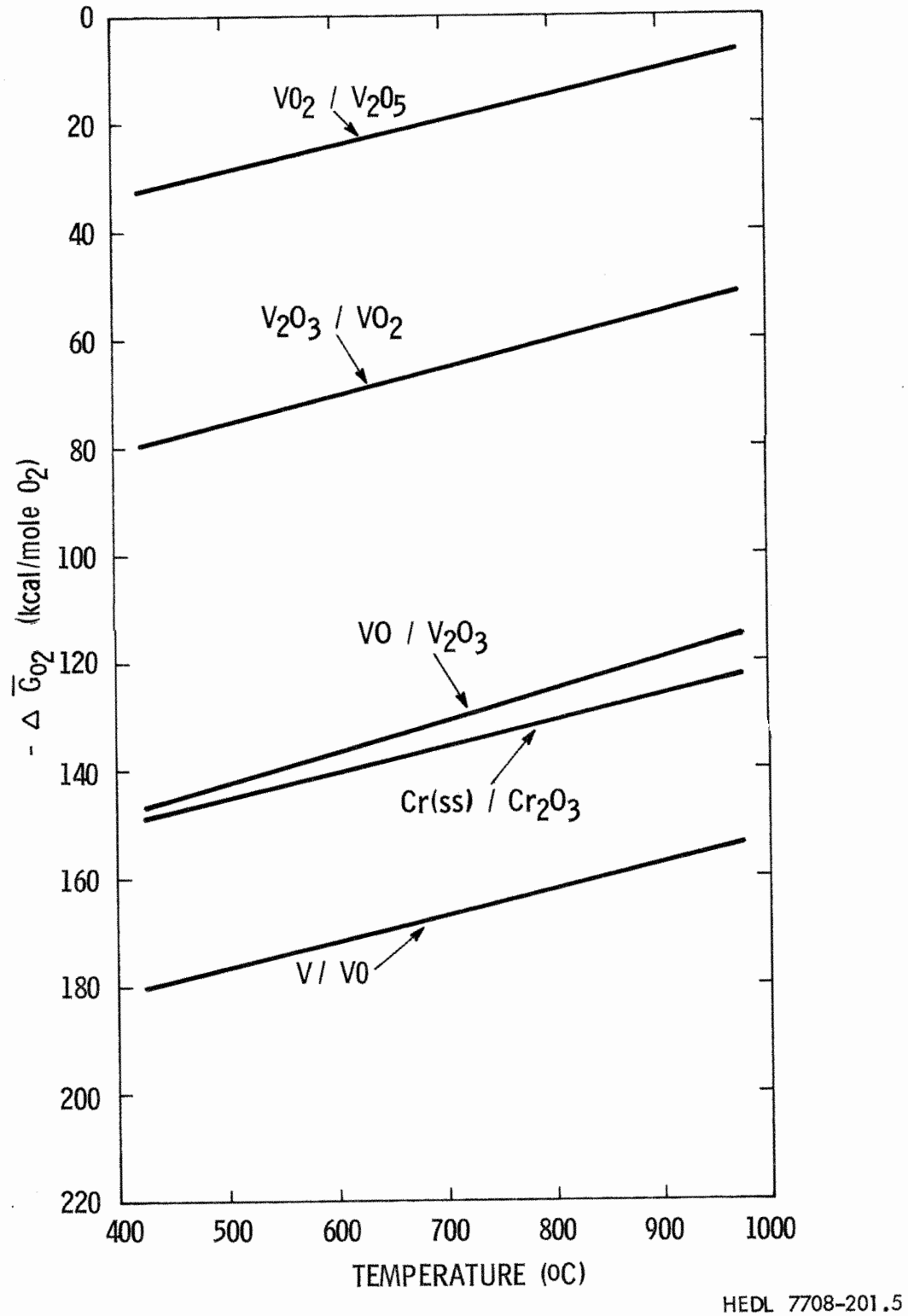

HEDL 7708-201.5

FIGURE 3

PHASE BOUNDARY OXYGEN POTENTIAL

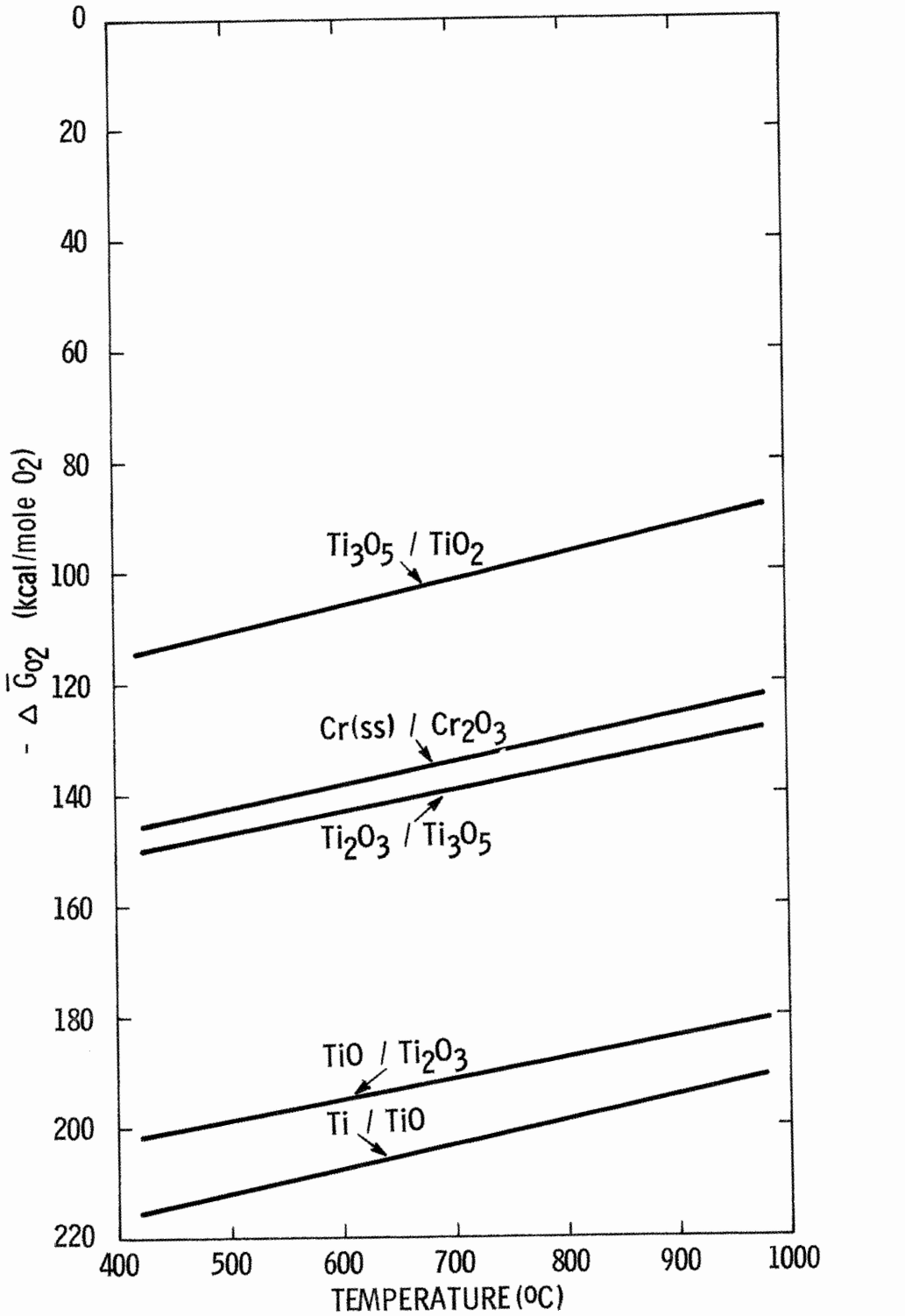

HEDL 7708-201.4

FIGURE 4

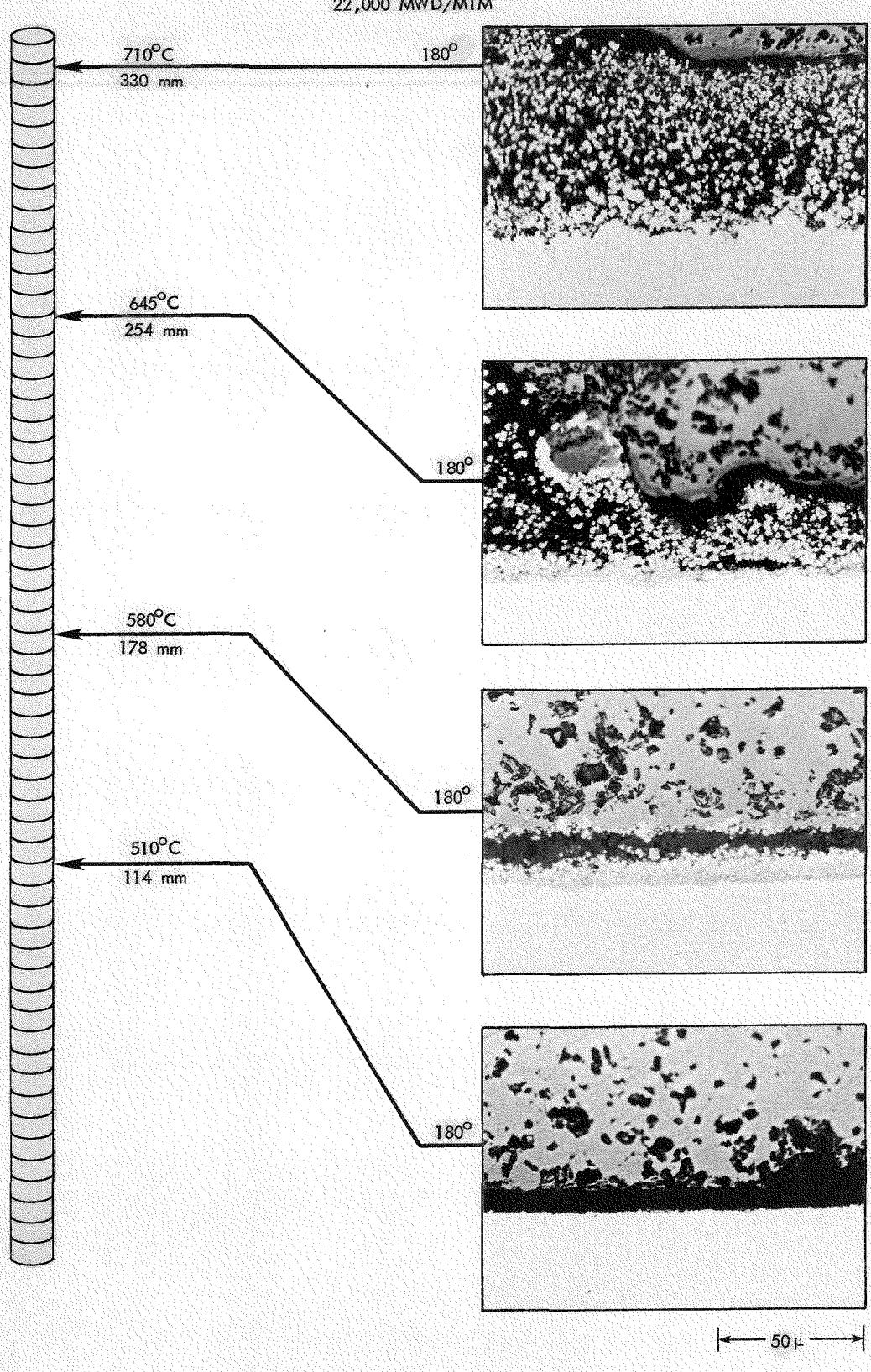
P-23B-S1
22,000 MWD/MTM
710°C
330 mm
180°
645°C
254 mm
180°
580°C
178 mm
180°
510°C
114 mm
180°
50 μ
HEDL 7704-59.3

FIGURE 5

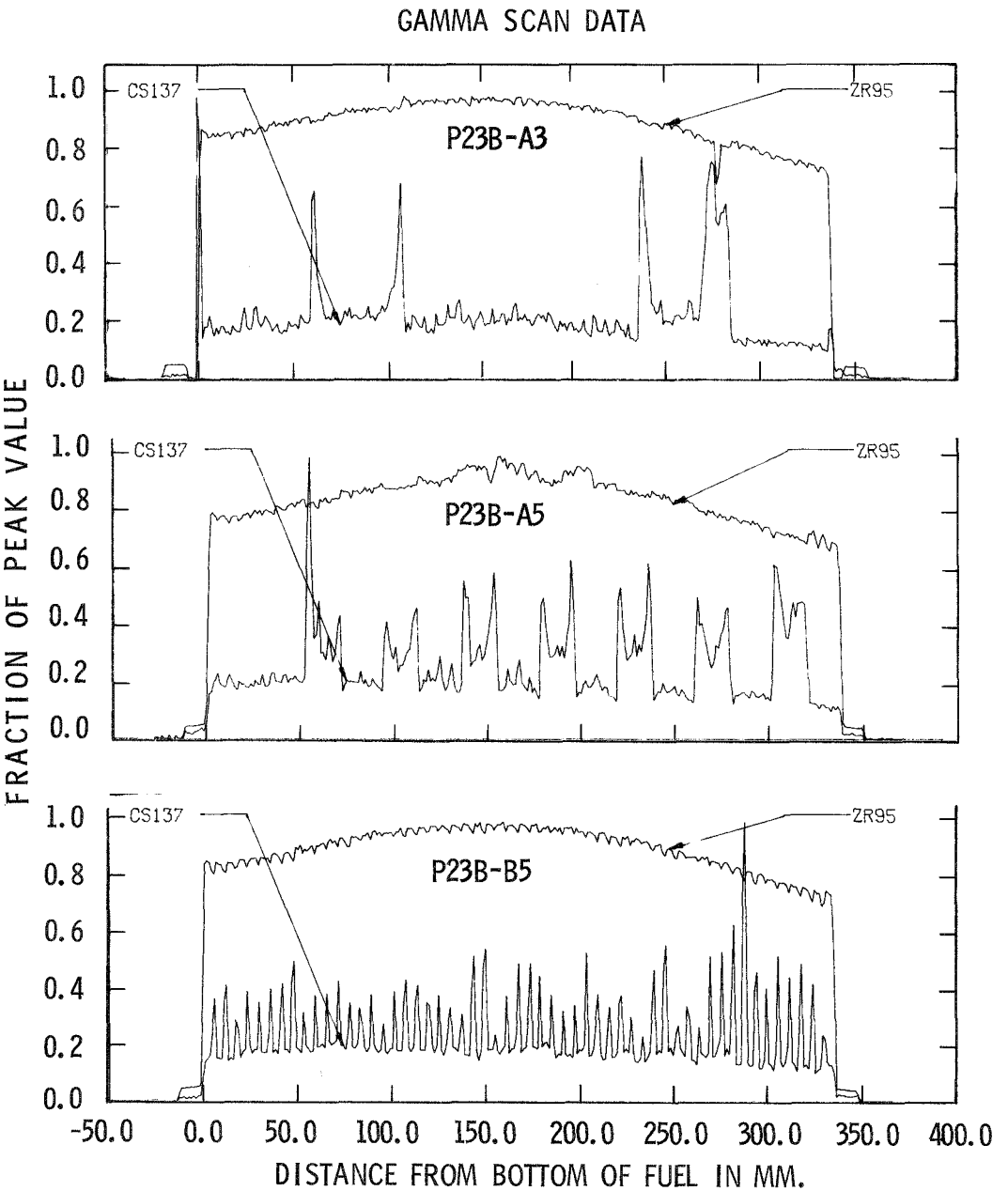

HEDL 7708-201.3

FIGURE 6

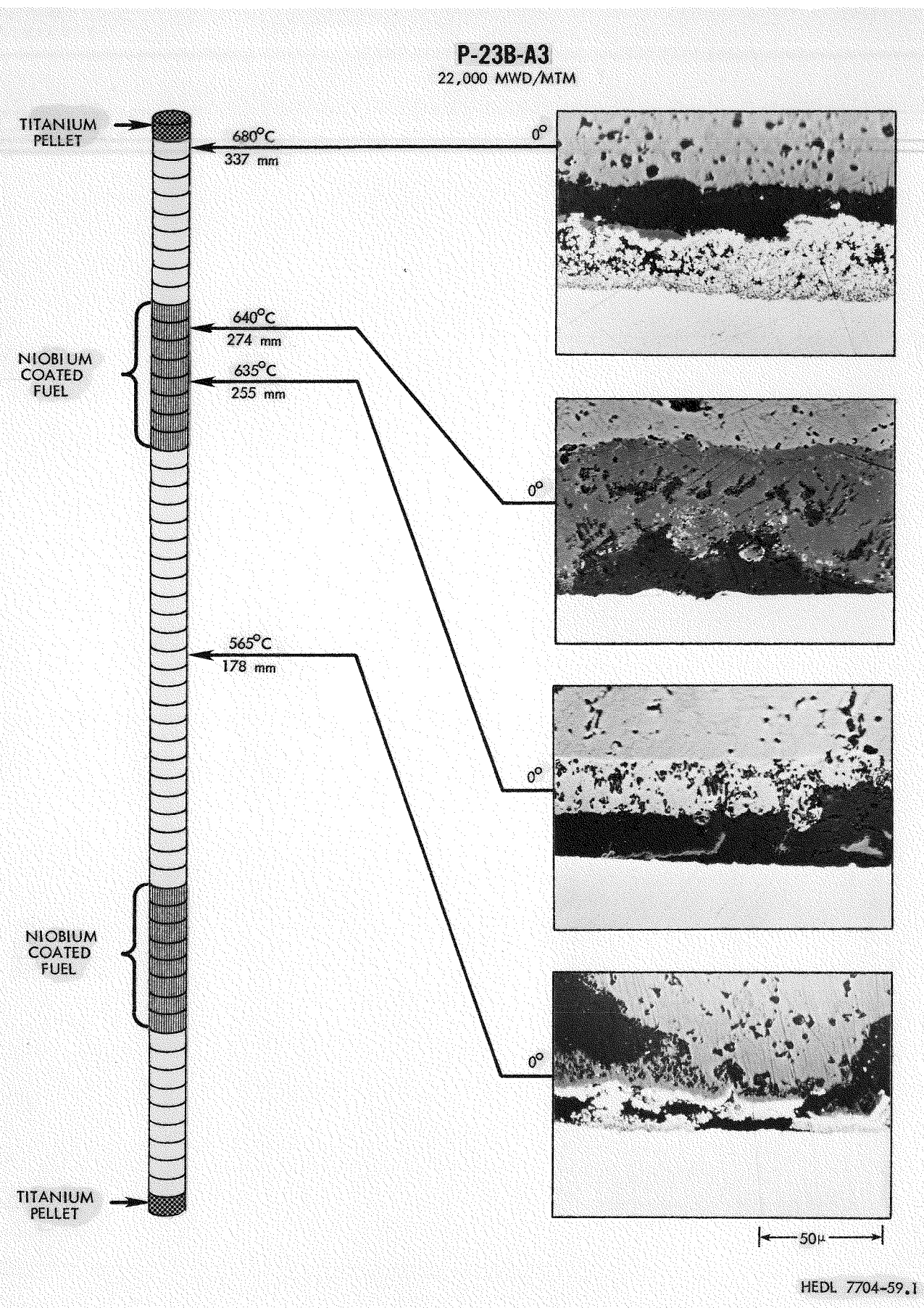
P-23B-A3
22,000 MWD/MTM
TITANIUM PELLET
680°C
337 mm
0°
640°C
274 mm
NIOBIUM COATED FUEL
635°C
255 mm
0°
0°
565°C
178 mm
NIOBIUM COATED FUEL
0°
TITANIUM PELLET
50μ
HEDL 7704-59.1

FIGURE 7

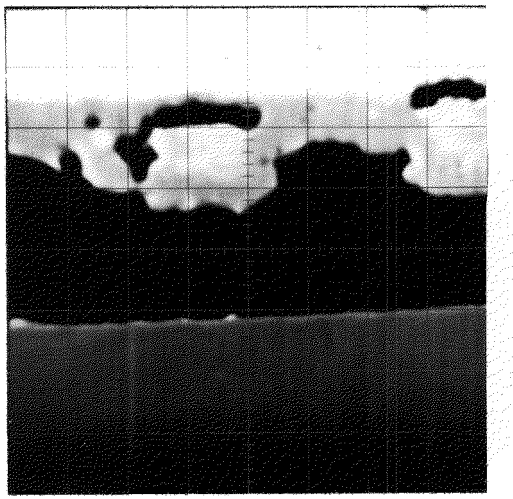

SPECIMEN CURRENT NEG 705-41

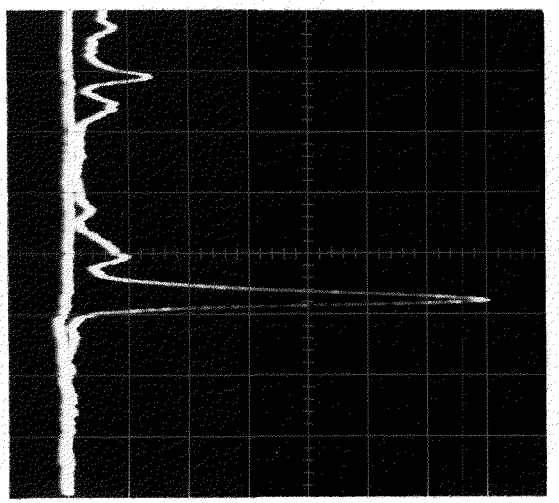

CESIUM NEG 705-43

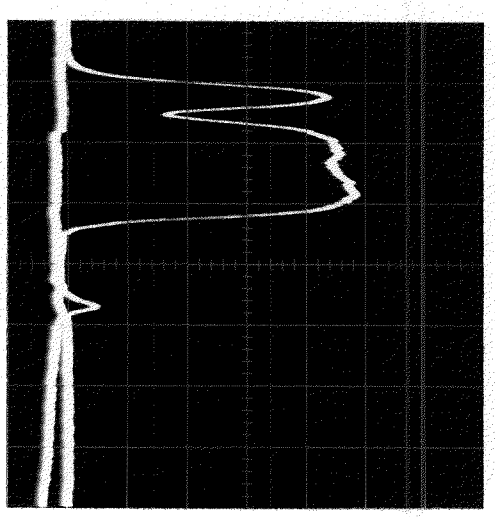

NIOBIUM NEG 705-42

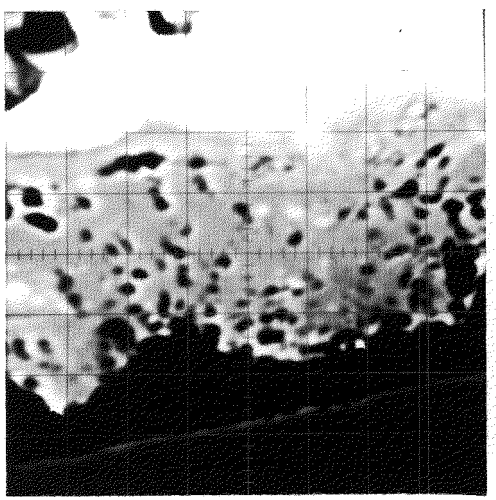

SPECIMEN CURRENT NEG 705-44

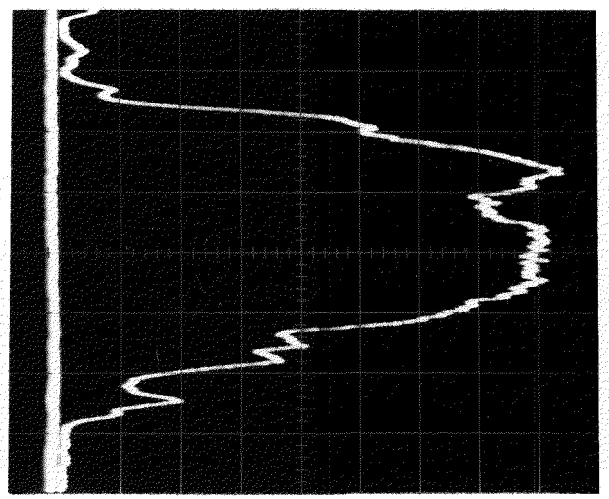

CESIUM NEG 705-46

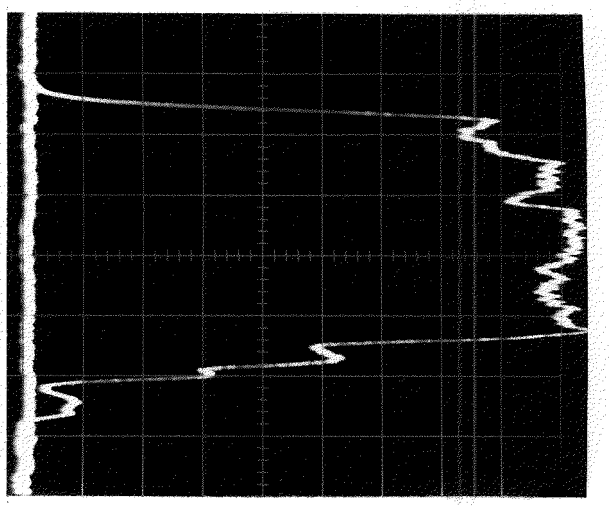

NIOBIUM NEG 705-45

FIGURE 8

80 μ

HEDL 7703-144.3

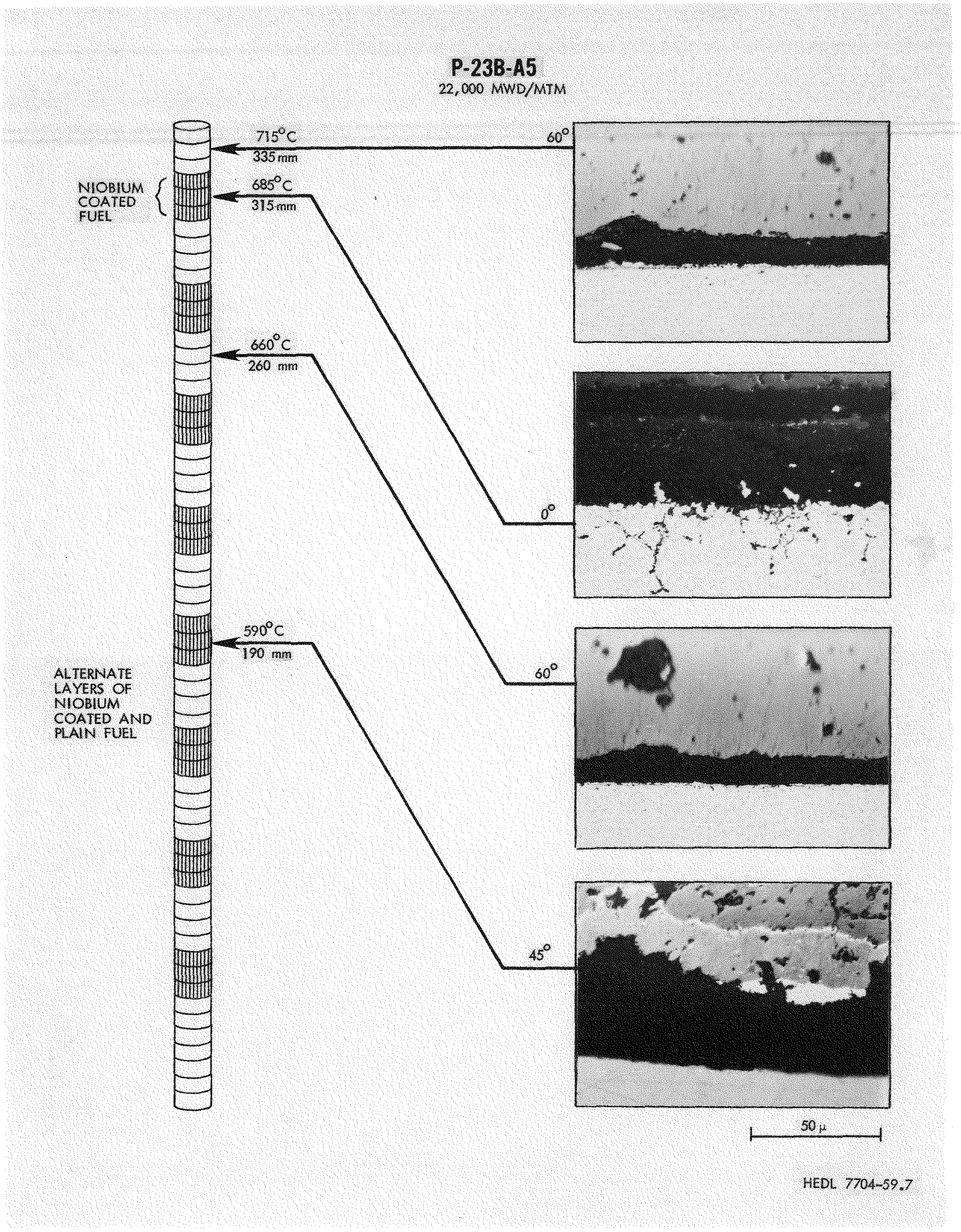
P-23B-A5
22,000 MWD/MTM
715°C
335 mm
685°C
315 mm
660°C
260 mm
590°C
190 mm
NIOBIUM COATED FUEL
ALTERNATE LAYERS OF NIOBIUM COATED AND PLAIN FUEL
60°
0°
60°
45°
50 μ
HEDL 7704-59.7

FIGURE 9

P-23B-A5-P

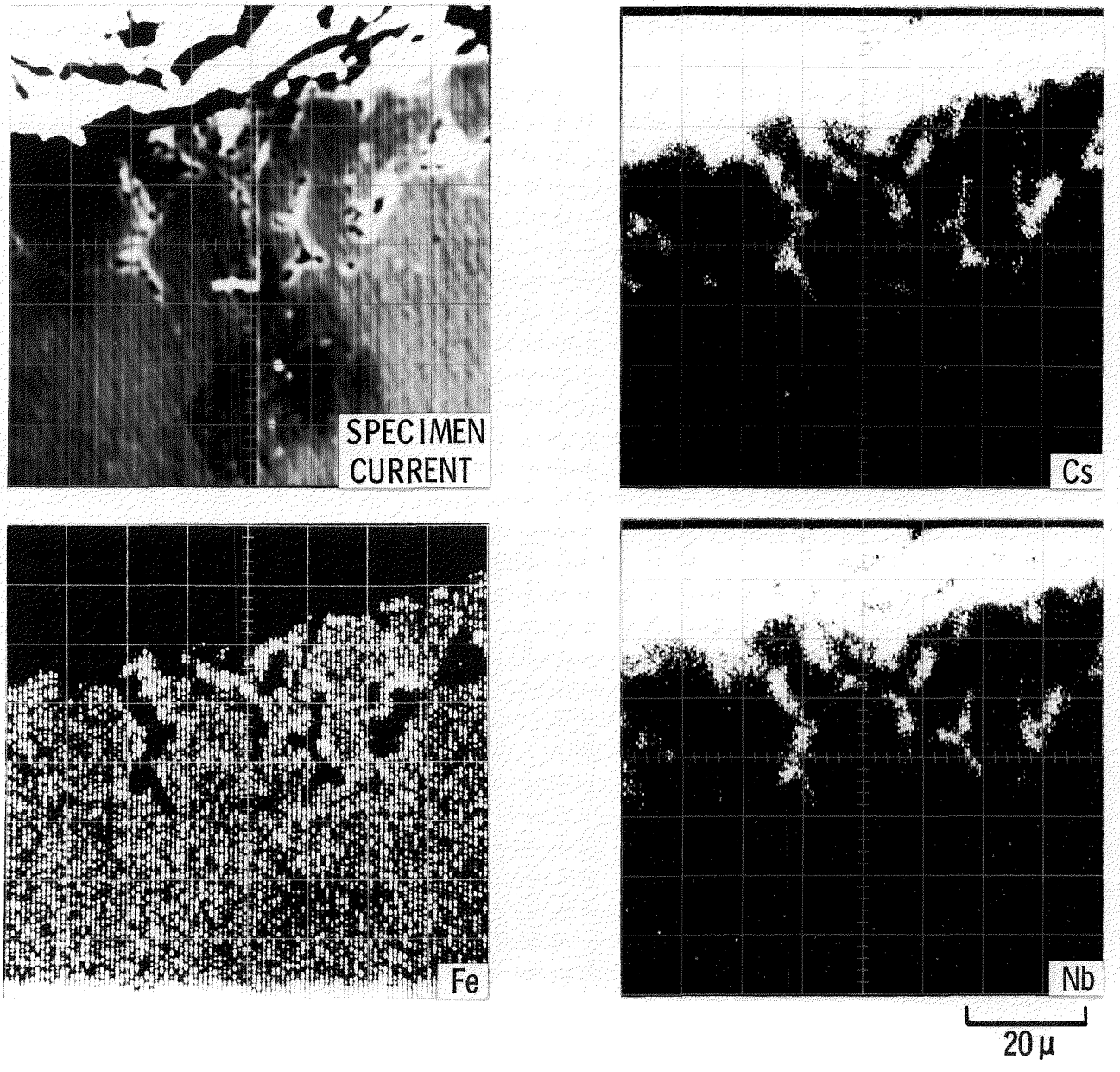

61

FIGURE 10

P-23B-B5

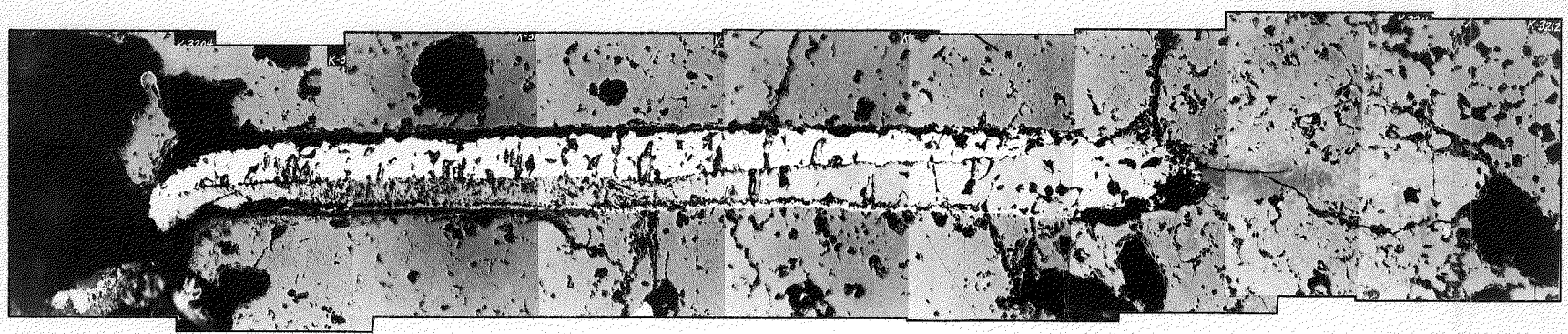

260 mm
120° ORIENTATION

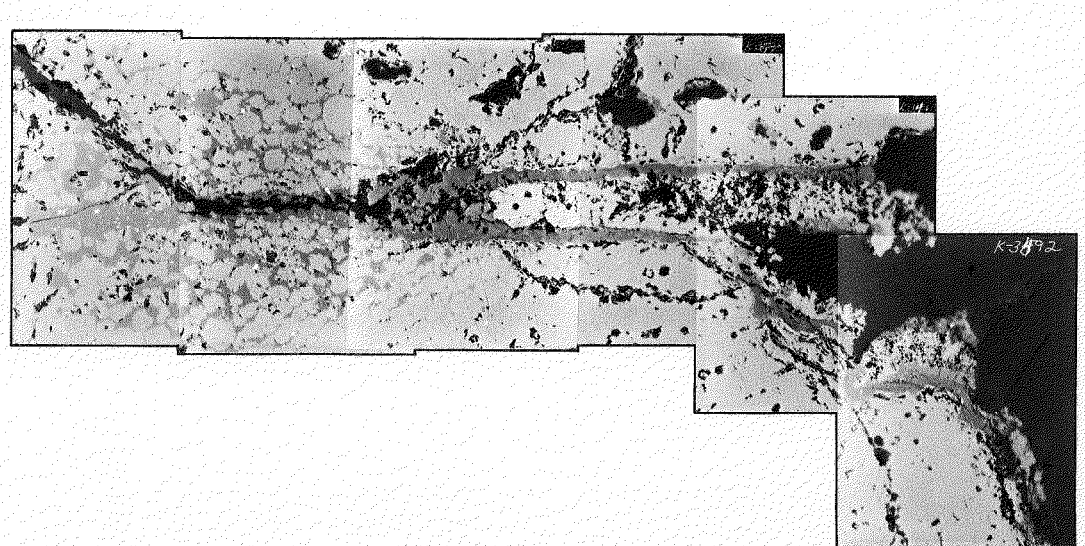

216 mm
300° ORIENTATION

FIGURE 11

GAMMA SCAN DATA

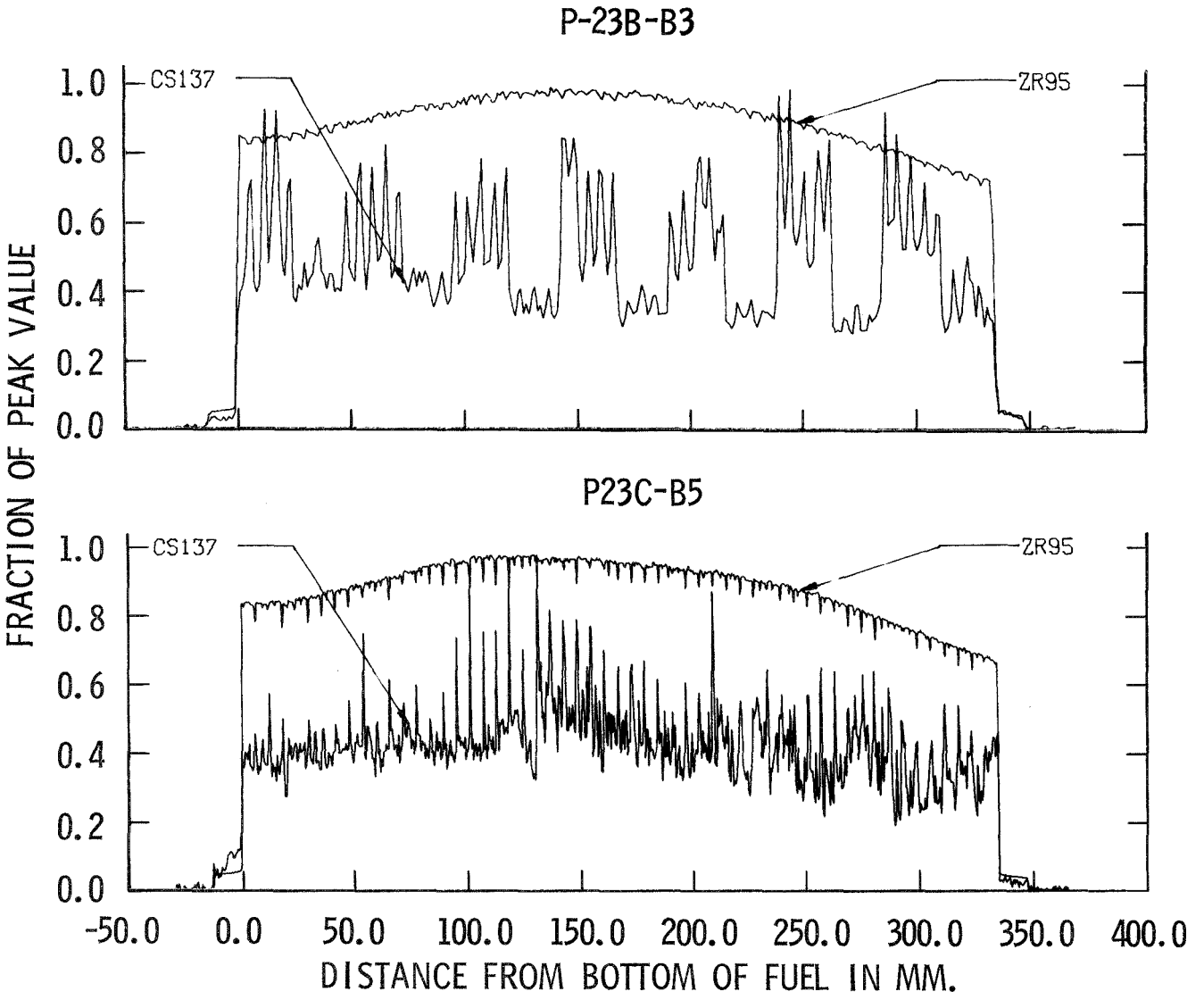

FIGURE 12

HEDL 7708-201.2

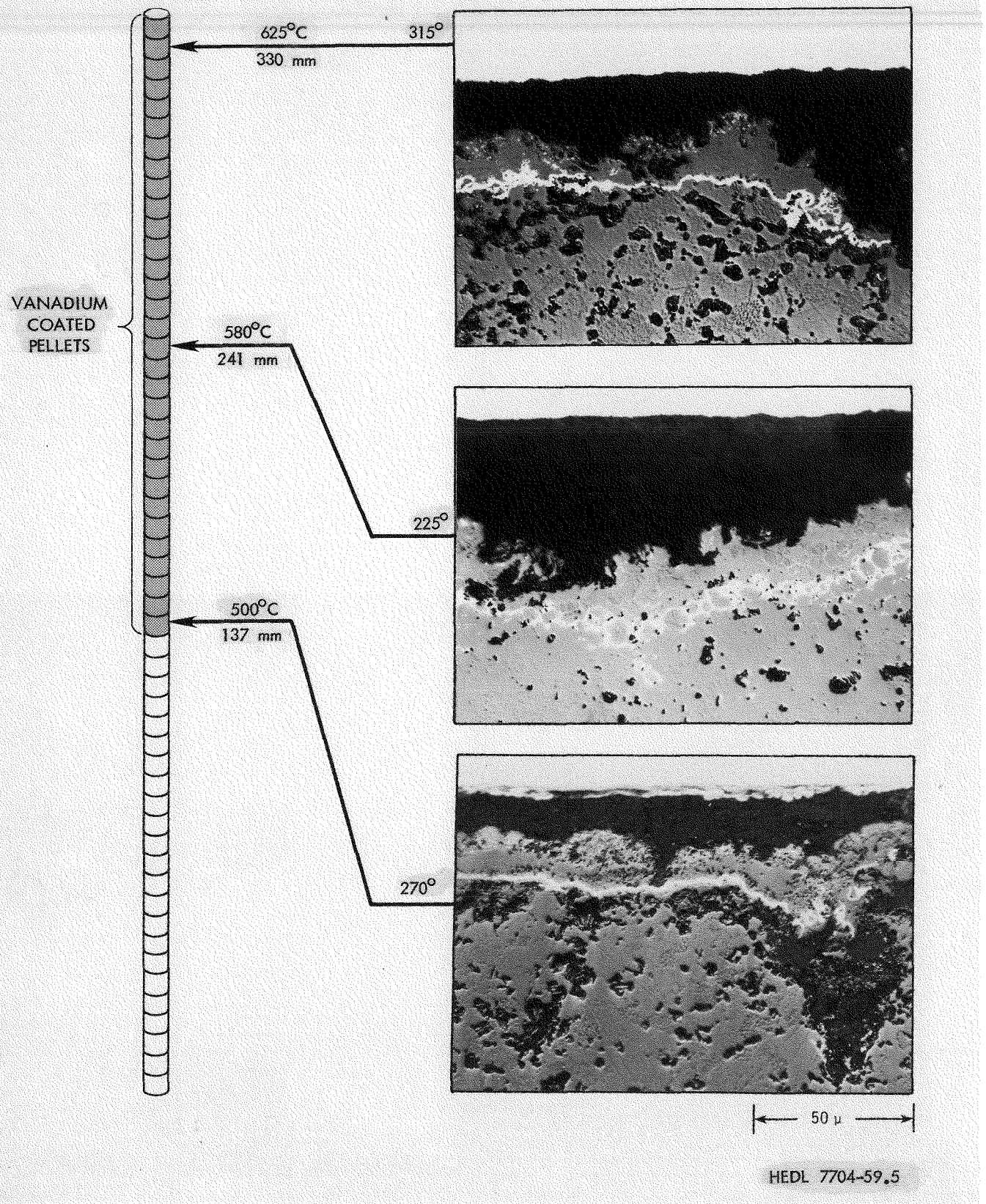
P-23C-B5
30,000 MWD/MTM
625°C
330 mm
315°
VANADIUM
COATED
PELLETS
580°C
241 mm
225°
500°C
137 mm
270°
50 μ
HEDL 7704-59.5

FIGURE 13

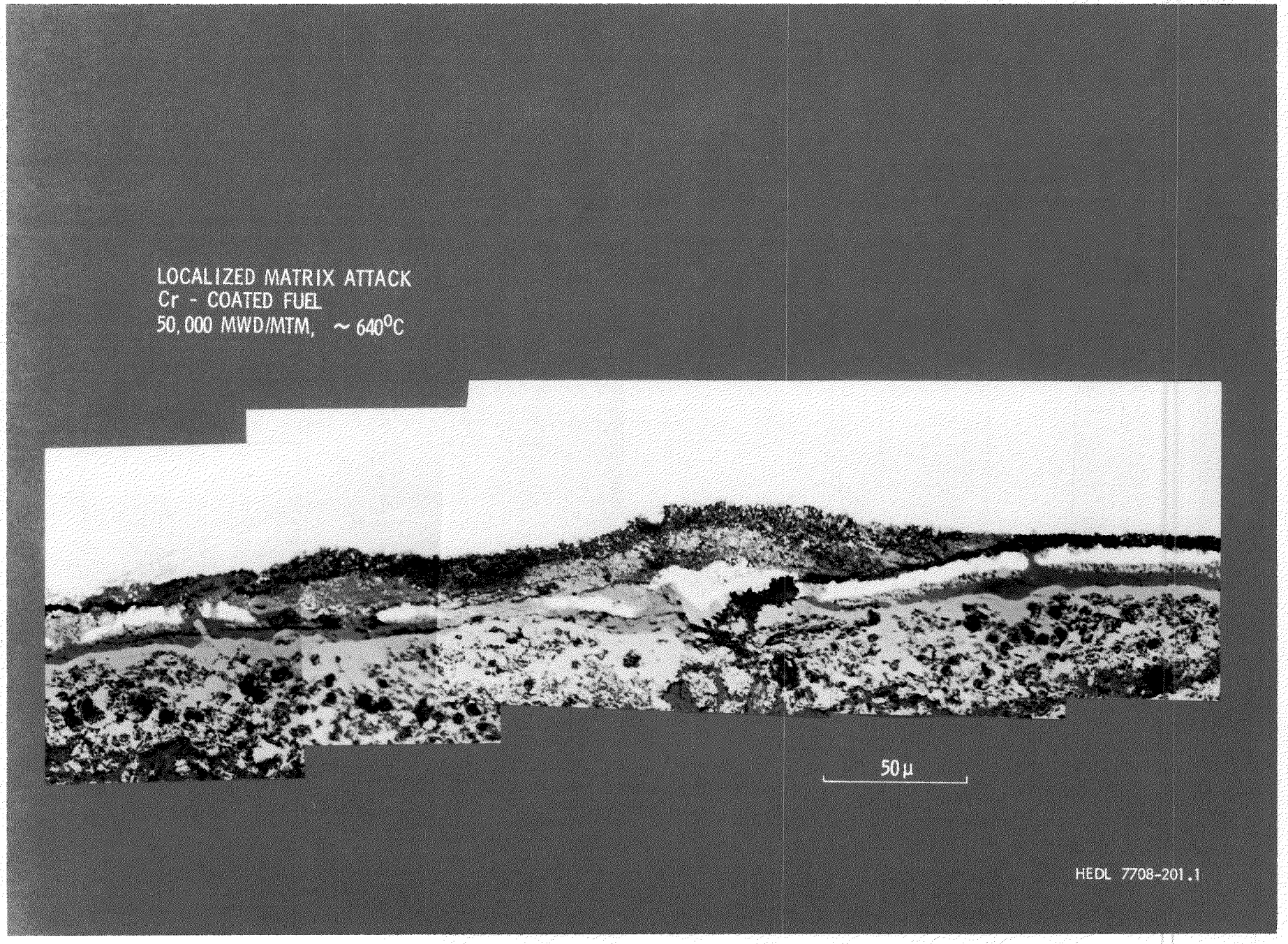
LOCALIZED MATRIX ATTACK
Cr - COATED FUEL
50,000 MWD/MTM, ~ 640°C
50 μ
HEDL 7708-201.1

FIGURE 14

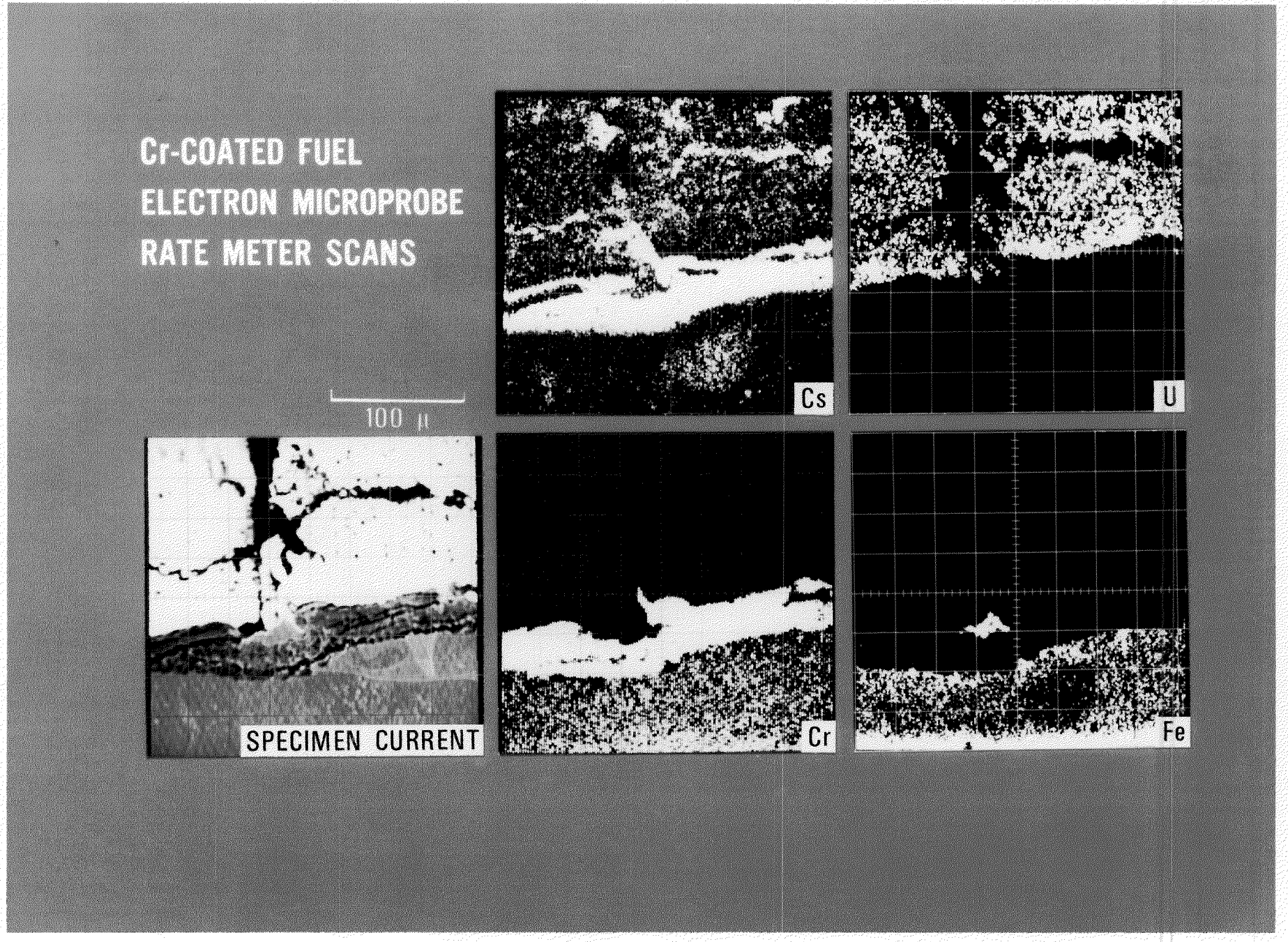
Cr-COATED FUEL
ELECTRON MICROPROBE
RATE METER SCANS
100 μ
Cs
U
SPECIMEN CURRENT
Cr
Fe

24

FIGURE 15

CONCLUSIONS

- CONTROL OF FCCI WITH BUFFER/GETTER MATERIALS APPEARS FEASIBLE
- BUFFER/GETTER MATERIALS MUST BE DISPERSED OVER FUEL COLUMN LENGTH TO BE EFFECTIVE
- AXIAL OXYGEN MOBILITY IS TO LOW FOR ISOLATED BUFFER/GETTER MATERIALS TO BE EFFECTIVE
- Nb, Ti AND Cr REACTED WITH Cs AFTER OXIDATION
  - SUGGESTED Cs AFFINITY RANKING: Nb>Ti>Cr>V

FIGURE 16